Ultrafast probe of magnetization dynamics in multiferroic $CoCr_2O_4$ and $Co_{0.975}Ge_{0.025}Cr_2O_4$

S. Parchenko,[1,2,3,*] N. Ortiz Hernández,[1] M. Savoini,[4] M. Porer,[1] M. Decker,[1] B. Burganov,[4] E. M. Bothschafter,[1] C. Dornes,[4] Y. W. Windsor,[1,5] M. Ramakrishnan,[1] L. Rettig,[1,5] M. Buzzi,[1] D. Schick,[6] K. Holldack,[6] N. Pontius,[6] C. Schüßler-Langeheine,[6] M. Radovic,[1] J. A. Heuver,[7] B. Noheda,[7] S. L. Johnson,[3,8] and U. Staub[1,†]

[1]*Swiss Light Source, Paul Scherrer Institut, 5232 Villigen, Switzerland*
[2]*Laboratory for Mesoscopic Systems, Department of Materials, ETH Zurich, 8093 Zurich, Switzerland*
[3]*Laboratory for Multiscale Materials Experiments, Paul Scherrer Institute, 5232 Villigen PSI, Switzerland*
[4]*Institute for Quantum Electronics, Eidgenössische Technische Hochschule (ETH) Zürich, Wolfgang-Pauli-Str. 16, 8093 Zürich, Switzerland*
[5]*Fritz Haber Institute of the Max Planck Society, Faradayweg 4-6, 14915 Berlin, Germany*
[6]*Helmholtz-Zentrum Berlin für Materialien und Energie GmbH, Albert-Einstein-Straße 15, 12489 Berlin, Germany*
[7]*Zernike Institute for Advanced Materials, University of Groningen, Nijenborgh 4, 9747AG, The Netherlands*
[8]*SwissFEL, Paul Scherrer Institut, 5232 Villigen, Switzerland*

(Received 1 April 2021; revised 1 December 2021; accepted 28 January 2022; published 25 February 2022)

We report on element-resolved ultrafast magnetization dynamics in multiferroic $CoCr_2O_4$ and $Co_{0.975}Ge_{0.025}Cr_2O_4$ after optical excitation above the electronic band gap. We observe demagnetization dynamics in the range of several picoseconds, up to two orders of magnitude faster than previously reported demagnetization in other ferrimagnetic insulators. Moreover, we find that the dynamics of the two magnetic ions differ significantly just below the Curie point. The dynamics of the low-temperature multiferroic phase are almost two times slower than those in the ferrimagnetic phase. This suggests that the additional magnetic cycloidal component, which is coupled to electric polarization at low temperatures, might influence the ultrafast magnetization dynamics.

DOI: 10.1103/PhysRevB.105.064432

I. INTRODUCTION

Controlling electronic or magnetic properties on ultrafast timescales by exciting materials with intense femtosecond laser pulses is an intensively discussed topic. This strong interest originates both from a fundamental question surrounding the physical processes taking place on picosecond and femtosecond time scales, as well as the potential for applications in data storage and manipulation. Magnetization reversal by ultrashort electromagnetic excitations with frequencies ranging from the visible to THz [1–7] has been demonstrated in selected metallic and dielectric materials. Furthermore, materials that have coupled magnetic and electric orders—multiferroics of type II [8]—open up new possibilities for simultaneous manipulation of the magnetization and electric polarization. This is possible because their macroscopic electric polarization is induced by magnetic order. One mechanism causing this magnetization-induced ferroelectricity is based on spin currents [9] driven by the Dzyaloshinskii-Moriya interaction (DMI) [10]. Although this mechanism is well understood in equilibrium, its nonequilibrium behavior and the corresponding dynamics of the different ferroic orders are not well established. Experiments on multiferroics have found strongly varying timescales for suppression of long-range magnetic order by laser excitations, spanning from 250 fs in cupric oxide [11] to several tens of picoseconds in orthorhombic $RMnO_3$ [12,13]. The origin of these differences in timescale is unclear. Expanding the study of magnetization dynamics to a broader range of multiferroics, in particular ones that harbor uncompensated ferrimagnetic order, may offer new insights on what sets the timescale of the magnetic order changes in response to intense optical excitation, in particular in the presence of uncompensated magnetic moments.

Cobalt chromite with the chemical formula $CoCr_2O_4$ (CCO) is a type-II multiferroic that exhibits a macroscopic magnetic moment and an electric polarization caused by significant magnetoelectric coupling [14]. CCO crystalizes in the normal spinel structure with two distinct crystallographic sites: tetrahedrally coordinated (A sites) and octahedrally coordinated (B sites) [15]. The Co^{2+} ions occupy A sites and the Cr^{3+} ions occupy B sites. CCO is a ferrimagnet below $T_C = 95\,\mathrm{K}$ with no magnetic compensation point and macroscopic magnetization along [001]. The magnetizations of the net Cr and Co magnetic sublattices are antiparallel, with the Co sublattice exhibiting larger moments at all temperatures. In addition, the Cr occupied B sublattice is a superposition of two magnetic sites B_1 and B_2 that have an antiparallel orientation of magnetic moments as well as different average canting angles [16].

Below $T_S = 27\,\mathrm{K}$ CCO undergoes a phase transition in which an additional long-range cycloidal spin modulation occurs with a propagation vector $k = (2/3\,2/3\,0)$ [14]. The

*Present address: European X-Ray Free-Electron Laser, Holzkoppel 4, 22869 Schenefeld, Germany; Corresponding author: sergii.parchenko@xfel.eu
†Corresponding author: urs.staub@psi.ch

resulting conical canting angle (defined by the ratio between the [001] component and the cycloidal component) is different for each sublattice [17] [see Fig. 1(d)]. Such magnetic spinel systems are often described through an effective unitless parameter u, for which different values indicate different magnetic configurations [18]:

$$u = 4J_{BB}S_BS_B/3J_{AB}S_AS_B. \quad (1)$$

Here J_{BB} and J_{AB} are the exchange coupling between B sites and between the A and B sites, respectively. The parameters S_A and S_B are the moments on these sites. The cycloidal component below T_S causes a loss of space inversion symmetry due to inverse DMI [14], enabling ferroelectricity. This strong magnetoelectric coupling allows a reversal of the polarization when magnetization is reversed by an external magnetic field. It is believed that the B sites are responsible for the spin conical state in spinels and the multiferroicity in CCO below T_S [19].

The equilibrium properties of CCO are known to vary significantly with in-plane strain, such that thin films differ from bulk [20]. A detailed study of the equilibrium magnetic properties in epitaxial thin films using soft x rays found a strong influence of strain on the coercive field and the magnetic ordering wave vector [21]. An additional path that was previously explored for engineering magnetic properties is doping with nonmagnetic Ge ions, which was found to induce an additional cycloidal component without significant changes of T_S and T_C [22]. Here, we investigate the ultrafast magnetization dynamics after optical excitation above the band gap in CCO films, where the coercive field changes from $H_c = 0.05$ kOe in bulk to $H_c = 20$ kOe in thin films. We find demagnetization times in the order of several picoseconds—much faster than expected for dielectrics. In addition, we reveal the possible influence of the coupling between spins and the lattice in the multiferroic state on the laser-induced magnetization dynamics and compare the dynamics in pure CCO and Ge-doped CCO.

II. EXPERIMENT

Thin epitaxial films of CCO and a Ge-doped CCO film were grown by pulsed laser deposition on [110]-oriented MgO. The pure CCO sample is the same as the one used in Ref. [21]. The Ge-CCO film was deposited at 600 °C in oxygen pressure of 1×10^{-3} mbar [21,22]. A KrF excimer laser with a 2-Hz repetition rate and a fluence of $\Phi = 1\,\mathrm{J\,cm^{-2}}$ was used. For the doped film, a Germanium doping of 0.025 per formula unit was selected by choosing a target for ablation with the stoichiometry of $Co_{0.975}Ge_{0.025}Cr_2O_4$ (Ge-CCO). The quality of the thin films was tested by reflection high-energy electron diffraction (RHEED) during the growth process. The Ge-CCO sample is the same as the one used in Ref. [22].

X-ray characterization of equilibrium magnetic properties was performed at the ReSoXS endstation [23] of the X11MA beamline [24] at the Swiss Light Source. The CCO sample was cooled in an in-plane magnetic field of ∼3 kOe from a

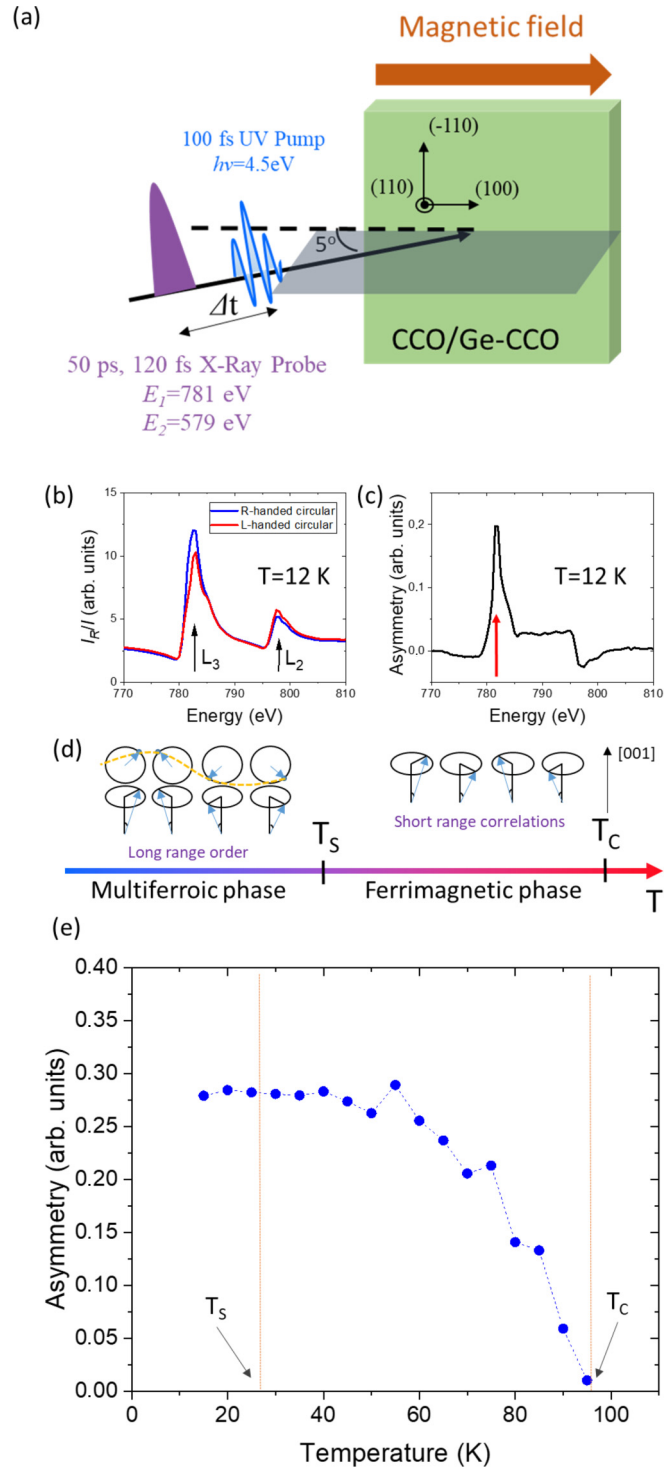

FIG. 1. (a) Sketch of the experimental geometry for the time-resolved pump-probe experiments. (b) X-ray reflectivity of CCO collected near the Co $L_{2,3}$ absorption edges using opposite circular polarization of incoming x rays at ReSoXS instrument at Swiss Light Source. (c) The corresponding XMCD asymmetry, calculated using Eq. (2). The red arrow indicates the x-ray energy with maximal contrast that has been selected for the time-resolved experiments. (d) Schematic description of the magnetic configuration in the different phases. (e) Temperature evolution of the asymmetry, reflecting the temperature dependence of the Co sublattice magnetization.

permanent magnet to ensure a monodomain magnetic state. Element-specific magnetization was measured using x-ray magnetic circular dichroism (XMCD) in reflection geometry, using a 5° incidence angle. Photon energies were used in the proximity of the Co $L_{2,3}$ edges, providing signals sensitive only to the Co magnetization [see Figs. 1(b) and 1(c)].

Time-resolved experiments were performed at the FemtoSpeX slicing facility at beamline UE56/1-ZPM of the BESSY II storage ring at HZB [25]. The experimental configuration, also for XMCD in reflection geometry, is sketched in Fig. 1(a). A magnetic field of $H = 2.5\,\mathrm{kOe}$ was generated by an electromagnet, and applied in the scattering plane, parallel to the sample's [001] in-plane crystal direction. Laser pulses with approximately 50 fs duration and energy of $E_{\mathrm{pump}} = 4.65\,\mathrm{eV}$ ($\lambda = 266\,\mathrm{nm}$) were used to excite the sample above band gap ($E_g = 3.23\,\mathrm{eV}$ [26]) at a repetition rate of 3 kHz. These pulses were obtained by third-harmonic generation of fundamental 800-nm light from a Ti:sapphire femtosecond laser. The pump beam was focused to a footprint of $150\,\mu\mathrm{m} \times 1720\,\mu\mathrm{m}$ on the sample surface. The incident fluence was kept fixed to $\Phi = 0.3\,\mathrm{mJ/cm^2}$ in all measurements to avoid laser excitation heating the sample above T_C and a possible effect of the excitation fluence variations on the obtained dynamics. The probe beam consisted of circularly polarized x rays with photon energies of either $E_1 = 781\,\mathrm{eV}$ or $E_2 = 579\,\mathrm{eV}$, corresponding to L_3 resonance energies of Co and Cr, respectively, and was used to selectively probe the magnetization of either the Co or the Cr sublattices. The probe spot size was approximately two times smaller than that of the pump, and its repetition rate was 6 kHz, allowing the measurement of an unperturbed signal in between every pumped signal. Two modes of x-ray pulses were employed: a regular mode, providing a temporal resolution of approximately 50 ps, and a slicing mode providing approximately 100-fs x-ray pulse lengths. The incidence angle for the pump and probe beams were 6° and 5° from the sample surface, respectively. The sample was cooled with a liquid helium flow cryostat to various temperatures below T_C. The lowest reachable temperature at the sample position was $T = 20\,\mathrm{K}$.

III. RESULTS

Energy-dependent reflectivity collected from the pure CCO film around the Co $L_{2,3}$ absorption edges for right-handed (C^+) and left-handed (C^-) circularly polarized incoming x rays are shown in Fig. 1(b) for a sample temperature of $T = 12\,\mathrm{K}$. To first order, the sublattice magnetization is proportional to the asymmetry given by

$$\frac{I_{H+}^{C+} - I_{H+}^{C-}}{I_{H+}^{C+} + I_{H+}^{C-}} = \frac{I_{H+}^{C+} - I_{H-}^{C+}}{I_{H+}^{C+} + I_{H-}^{C+}} \propto M_{\mathrm{Co}}, \tag{2}$$

where I is the intensity of reflected x rays, $C+(-)$ indicates the handedness of the incoming circular polarization, and $H+(-)$ is the sign of the external magnetic field H. Note that XMCD at the transition metal L edges are probing the difference between the occupation of the spin up and spin down bands. The contrast achieved by reversing the magnetization is therefore equivalent to the more conventional practice of changing the handedness of the circular polarization [27].The respective XMCD energy dependence is presented in Fig. 1(c). An XMCD contrast [Eq. (2)] of up to 20% was observed. The Co $L_{2,3}$ absorption edges correspond to electronic excitations from occupied $2p$ core states into the partially occupied $3d$ states through an electric dipole transition and thus contain information on the Co sublattice's $3d$ magnetization [28].

Similar to XMCD in absorption mode, reflection-mode XMCD probes the magnetization component projected onto the wave vector k of the incident x rays. There are, however, some important differences between the two. While absorption-mode XMCD directly measures helicity-dependent changes in the imaginary part of the refractive index, reflection-mode XMCD depends on helicity-dependent changes in both the real and imaginary components of the refractive index. In addition, the energy dependence in reflection mode is further complicated by the contribution of resonant and nonresonant reflectivity. These complications make sum rule analyses impractical to apply to reflectivity, but the advantage of reflectivity is that it simplifies ultrafast measurements in the time domain.

The temperature evolution of the XMCD signal taken using 781-eV photons (where Co L_3 XMCD contrast is maximal) is presented in Fig. 1(e). Assuming that the spin and orbital magnetic moments have equal temperature dependences [21], the plot represents the temperature evolution of the Co sublattice magnetization, to first order, which follows a regular order parameter behavior [21] that can be roughly described by a Brillouin function. Similar behavior is exhibited by the signal at the Cr edge, with the opposite sign [21]. The macroscopic magnetization exhibits a complicated temperature dependence as it is the superposition of these two antiparallely ordered sublattices [29].

Figure 2(a) presents the demagnetization of pure CCO following a fs laser excitation at various initial temperatures. The data were collected using XMCD contrast in regular mode (50 ps resolution). All transient signals are normalized to the equilibrium XMCD contrast measured at the saturation magnetization of the respective temperature [see Fig. 1(e)]. Absorption from above-band-gap excitation leads to an efficient laser-induced demagnetization process, as the initial drop of magnetization is limited only by the 50-ps resolution, and then recovers on a nanosecond time scale. Notably, at 2 ns delay the magnetization recovers approximately half of the initial drop, independent of the initial temperature. The time trace taken at $T = 50\,\mathrm{K}$ exhibits a somewhat smaller quenching amplitude. We interpret this as an experimental artifact possibly caused by small sample drifts between different temperatures and/or ice condensation. Figures 2(b) and 2(c) present transient XMCD contrast collected at the Cr and Co edges in slicing mode (100 fs resolution) near T_C at $T = 85\,\mathrm{K}$. The observed demagnetizations are different for the two magnetic sublattices and are much faster than in other insulating compounds [30], where demagnetization takes hundreds of ps when excited with comparable excitation fluences. The time-resolved XMCD signal was fit to the function

$$M/M_0 = y_0 + Ae^{-t/\tau}, \tag{3}$$

where τ and A are the demagnetization time constant and amplitude, respectively. The best fits yielded time constants of

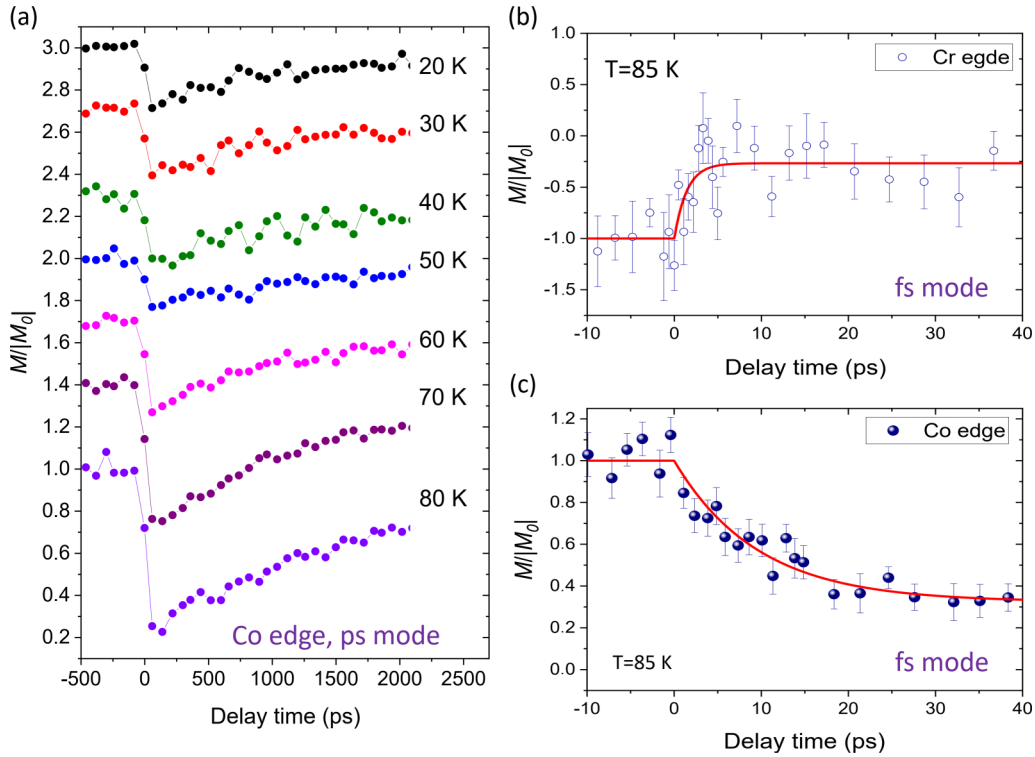

FIG. 2. (a) Demagnetization dynamics of the pure CCO film, collected in ps mode at several temperatures using XMCD contrast near the Co L_3 edge. The scans are vertically shifted for visibility. (b), (c) Demagnetization dynamics at $T = 85$ K, which is close to $T_{C=95\,\mathrm{K}}$, collected in slicing mode at the Cr and Co L_3 edges, respectively.

$\tau_{\mathrm{Co}} = (9.5 \pm 1.2)$ ps and $\tau_{\mathrm{Cr}} = (1.1 \pm 1.5)$ ps for the Co and Cr sublattices, respectively. Despite the lower signal-to-noise ratio at the Cr edge, the dynamics of the sublattices clearly differ by almost one order of magnitude.

We now compare the dynamics in pure CCO with those in Ge-CCO. The Ge-CCO sample clearly exhibits different long-range order and increased magnetic anisotropy due to strain (see Ref. [22]). Figure 3 presents a direct comparison of demagnetization dynamics from pure and Ge-doped CCO taken at the Co edge in slicing mode and, at several initial temperatures. The transient magnetization values are normalized to the equilibrium values at the respective temperatures. For both systems we compare the demagnetization dynamics in the multiferroic phase (data at $T = 20$ K) with those of the ferrimagnetic phase ($T = 35$ K, $T = 65$ K). With decreasing temperatures, the demagnetization becomes faster in comparison to those very close to T_C [Fig 2(c)]. This behavior is consistent with previous observations [31–36] and has been attributed to critical slowing down near T_C.

The best fits to Eq. (3) are shown as red lines in Fig. 3. Figure 4 presents the extracted demagnetization times constants and amplitudes. In the ferrimagnetic phase above T_S, the time constant is ∼2 ps for both samples, with Ge-CCO being slightly faster.

In the multiferroic phase, we find significantly stronger demagnetization amplitudes for Ge-CCO, but for both systems demagnetization is slower in this phase [Fig. 4(a)]. This reaches a factor of 2 for pure CCO, while the net magnetization of Co sublattice is almost the same for the two phases at $T = 20$ K and $T = 35$ K [see Fig. 1(e)]. The relative magnetization drop at $\Delta t = 15$ ps is shown in Fig. 4(b). We adopt a model assuming that at $\Delta t = 15$ ps, the Co spin system already thermalizes to an effective temperature T_S^{Co}. Next, we use the temperature dependence of the equilibrium XMCD [Fig. 1(e) above and the data underlying Fig. 4(c) in Ref. [22], for CCO and Ge-CCO, respectively] to calculate effective temperature changes in the magnetic system for Co sublattice ΔT_S^{Co}, shown in Fig. 4(b). Here we present the relative change of the magnetization of Co sublattices, normalized to its absolute value in equilibrium at a given temperature. The obtained ΔT_S^{Co} trend differs between CCO and Ge-CCO. The measured effective magnetization suppression ΔM between temperatures is, however, normalized to the unpumped XMCD value at a given temperature. This means that we are comparing relative (not absolute) XMCD changes. Note also that the comparison of time traces in ps and slicing mode is not straightforward as the limited time resolution in ps mode affects the overall dynamics acting as a low pass filter.

Figure 5 presents the Co transient magnetization in CCO at $\Delta t = 20$ ps, normalized to unpumped values, as a function of incident fluence, for initial temperatures below and above the multiferroic transition. The signal begins to saturate above approximately $\Phi = 0.45\,\mathrm{mJ/cm^2}$ for both cases. The fluence dependence observed at initial temperatures of $T = 20$ K and $T = 35$ K is clearly different. In the ferrimagnetic phase magnetization suppression gradually approaches a nearly constant value upon increasing the laser fluence. For data taken in the multiferroic phase we observe a deviation from this dependence up to $\Phi = 0.35\,\mathrm{mJ/cm^2}$ (see inset to Fig. 5). The magnetization suppression is slightly smaller than

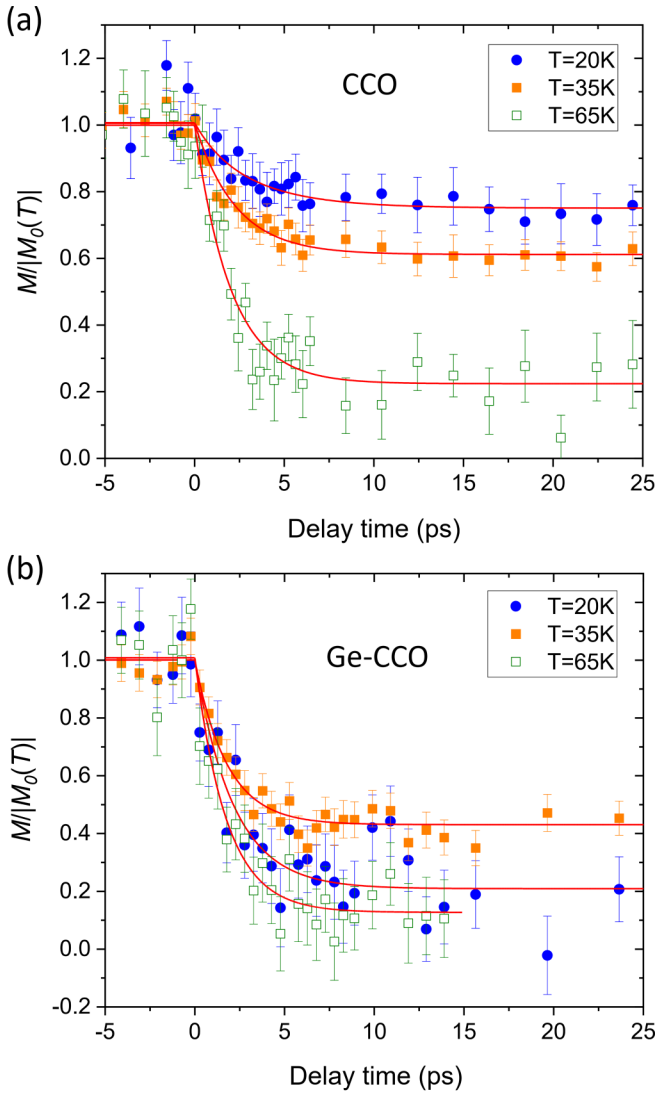

FIG. 3. Demagnetization dynamics of the Co sublattice for $CoCr_2O_4$ (a) and Ge-doped $CoCr_2O_4$ (b) at several initial temperatures and an excitation fluence $\Phi = 0.3\,\mathrm{mJ/cm^2}$. The red lines represent the best fit to Eq. (3).

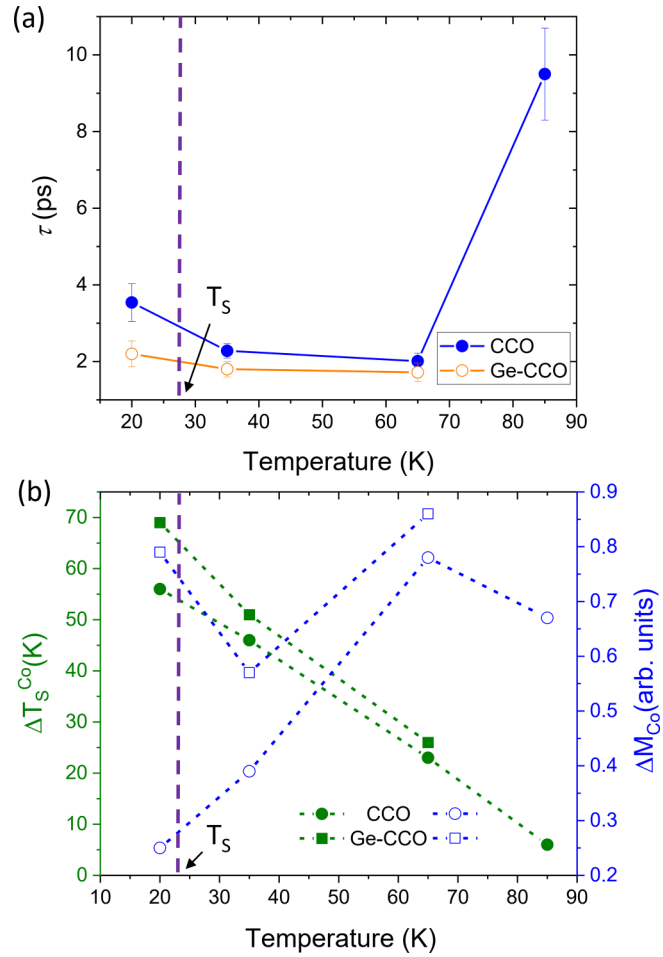

FIG. 4. (a) Demagnetization decay times τ for $CoCr_2O_4$ and Ge-$CoCr_2O_4$ at several temperatures. (b) An extracted temperature change of the spin system (left axis) compared to the relative suppression in the XMCD signal (right axis).

in Fig. 4, but has the same trend for that particular fluence. This suggests that additional energy is required for ultrafast suppression of the magnetic cycloid in the multiferroic phase. It is clear that when pumped with sufficiently high fluence, the material may be already in the paramagnetic state at $\Delta t = 20\,\mathrm{ps}$. In this scenario we would expect both curves to reach zero. The small remaining magnetization in the experimental data may indicate that a portion of the film near the substrate is not sufficiently pumped due to the limited penetration depth at the excitation wavelength.

IV. DISCUSSION

In general, the rate of laser-induced magnetization suppression in dielectrics is proportional to the magnetic anisotropy [37]. Energy transfer from electrons to lattice and then to spins happens faster in materials with large spin-orbit coupling. With a nonzero orbital magnetic moment at Co and Cr sublattices, CCO and Ge-CCO have a large magnetocrystalline

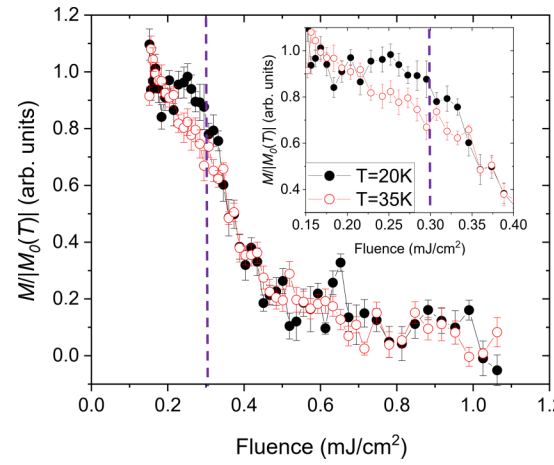

FIG. 5. Normalized transient magnetization in pure CCO as a function of pump fluence for initial temperatures of $T = 20\,\mathrm{K}$ (multiferroic phase) and $T = 35\,\mathrm{K}$ (ferrimagnetic case), measured at 20 ps delay time. The violet dashed lines indicate the laser fluence used for the delay scans shown in Figs. 2 and 3, and the inset is a closeup around this value.

anisotropy [21] which is further increased in our thin films due to strain [38]. Correspondingly, these films exhibit very large coercive fields, particularly at low temperatures. Furthermore, implanting nonmagnetic Ge ions creates local defects that change the crystal field and lead to a further increase in magnetic anisotropy [22]. The faster demagnetization observed in Ge-CCO is consistent with these considerations.

A second consideration is that the optical excitation injecting electrons into the conduction band by above-band-gap excitation. This enables spin-flip scattering which is responsible for ultrafast demagnetization in metals, typically occurring within a few hundreds of femtoseconds [39]. Density functional theory (DFT) calculations [40,41] have shown that in the energy range above E_F accessible with our excitation there are more unoccupied Cr states than Co states. Therefore, the efficiency of exciting Cr ions is larger than that for Co ions, which can explain the faster magnetization dynamics observed for the Cr sublattice (Fig. 2). Thus there appear to be two mechanisms contributing to the demagnetization process in our experiments: (i) direct spin-lattice coupling mediated by spin-orbit coupling, and (ii) spin-flip scattering from highly excited electronic states enabled by the above-band-gap excitation.

Compared to CCO, Ge-CCO reacts faster to the ultrafast laser excitation, and with a larger drop in magnetization. The larger changes in spin temperatures for lower initial temperatures are in good agreement with data obtained in the picosecond mode [see Fig. 2(a)]. A possible explanation for the relative magnetization reduction after the laser excitation at different initial temperatures and their recovery dynamics might arise from the temperature dependence of the heat capacity, as argued for other materials [34]. Thus, optical excitation at low temperatures leads to stronger effective temperature changes [see Fig. 4(b)]. Taking into account the temperature dependence of the magnetization [Fig. 1(e)], we expect larger changes in spin temperature for low initial temperatures.

Nevertheless, demagnetization time differences close to an order of magnitude between the antiferromagnetically coupled Co and Cr magnetic sublattices (Fig. 2) is rather surprising as it is usually expected that strong magnetic exchange couplings should equilibrate the dynamics on a sub-ps timescale. A similar phenomenon was observed in some rare-earth transition metals (RE-TM) alloys [42,43] or oxides with TM and weakly coupled $4f$ magnetic ions [44]. In these cases, the observed difference in the demagnetization time scale of the RE and TM sublattices was much smaller and could be explained by specifics of $3d$ and $4f$ magnetism [45]. Decoupled states between the sublattices in the time domain could be attributed to a specific value of the parameter u [see Eq. (1)]. For CCO, $u > 2$, which means that the intrasublattice coupling constant of B sites J_{BB} is stronger than the intersublattice antiferromagnetic coupling constant between A and B sites J_{AB}. In ferrimagnets, the intersublattice exchange interaction tends to equilibrate the different sublattices. In our case $J_{BB} > J_{AB}$, thus this equilibration is slower than the demagnetization of the Cr. This shows that the triangular magnetic configuration with exchange couplings described by parameter u, crucial for the multiferroic state, is directly correlated with the ultrafast magnetization dynamics.

In the multiferroic phase, magnetoelectric coupling between electrons, spins, and the lattice is expected to increase the efficiency of energy transfer from electrons to spins, increasing demagnetization speed. In contrast, the observed dynamics seem to slow down in the multiferroic phase [Fig. 4(a)]. This might be caused by the additional antiferromagnetic cycloidal component induced at T_S. The magnon spectrum is expected to shift to higher energies in the multiferroic phase [46–49], resulting in fewer excitations available to dissipate the energy. While uncompensated moments could be quenched more efficiently by scattering with low energy excitations, the antiferromagnetic spin components may lack the respective magnon or phonon modes to dissipate the energy. In CCO these two orders are coupled, allowing magnetic field-induced reversal of electric polarization [14]. An alternative scenario could be that the increase of demagnetization time is due to the critical slowing down effect of the AFM component near the T_S transition, similar to the effect observed for the ferrimagnetic component at $T = 85$ K. While testing this hypothesis would require additional data, we believe that the contribution of critical slowing down is likely to be minor as the sublattice magnetization of Co sublattice is almost unaffected at T_S and only a small fraction of the Co moment contributes to the long-range antiferromagnetic order.

Last, we consider the demagnetization amplitudes in the multiferroic phase. On the one hand, results presented in Fig. 5 confirm that higher fluencies are required to suppress the magnetization compared to the ferrimagnetic phase. On the other hand, demagnetization amplitudes are larger Ge-CCO compared to pure CCO. This may relate to an increased magnetic anisotropy, which might affect the efficiency of demagnetization upon laser excitation and thus lead to stronger XMCD suppression. However, as already pointed out before, more experimental data would be required to consolidate such a scenario. The role we attribute to the long-range order remains somewhat speculative, but can be directly tested with pump-probe measurements on the AFM (2/3 2/3 0) reflections, which probe the dynamics of the cycloidal component, and are directly accessible at the Co L_3 edge. Such an experiment is rather challenging due to the low intensity of the (*qq0*) peak [21] and requires today an XFEL.

V. SUMMARY

In summary, we studied element-specific ultrafast demagnetization dynamics of multiferroic $CoCr_2O_4$ and Ge-doped $CoCr_2O_4$ upon above-band-gap excitation. The observed magnetization suppression occurs within several picoseconds, which is fast compared to other dielectrics. The demagnetization of the Co and Cr sublattices are significantly different near the Curie temperature. This unexpended finding is attributed to the dominant exchange coupling within the Cr sublattice compared to the weaker Co-Cr interaction. In addition, the available data hint at a demagnetization time in the multiferroic phase being two times larger than just above T_S. This change might be attributed to the appearance of the additional antiferromagnetic cycloidal component below T_S. At the same time, observed changes could be also due to the critical slowing down near the multiferroic phase transition.

Experimental and fit data are accessible from the PSI Archive [50].

ACKNOWLEDGMENTS

We gratefully thank the X11MA beamline staff for their experimental support. The financial support of the Swiss National Science Foundation and its National Center of Competence in Research, Molecular Ultrafast Science and Technology (NCCR MUST) Grant No. 51NF40-183615 is acknowledged. M.R. acknowledges the financial support of the Swiss National Science Foundation (SNSF) (Sinergia project "Toroidal moments") Grant No. CRSII2_147606, N.O.H. and M.D. from SNSF Grant No. 200021_169017, and Y.W.W. from Grant No. 200020_159220. M.R. was supported by SNSF Research Grant 200021_182695. E.M.B. acknowledges funding from the European Community's Seventh Framework Programme (FP7/2007-2013) under Grant Agreement No. 290605 (PSI-FELLOW/COFUND). Also acknowledged is support by the National Center of Competence in Research, Materials' Revolution: Computational Design and Discovery of Novel Materials (NCCR MARVEL). The research leading to this result has been supported by the project CALIPSOplus under Grant Agreement No. 730872 from the EU Framework Programme for Research and Innovation Horizon 2020. This work received funding from the DFG within the Emmy Noether program under Grant No. RE 3977/1, and within the Transregio TRR 227 Ultrafast Spin Dynamics (Projects A09 and A03). We thank HZB for the allocation of synchrotron radiation beamtime.

[1] T. A. Ostler, J. Barker, R. F. L. Evans, R. W. Chantrell, U. Atxitia, O. Chubykalo-Fesenko, S. El Moussaoui, L. Le Guyader, E. Mengotti, L. J. Heyderman, F. Nolting, A. Tsukamoto, A. Itoh, D. Afanasiev, B. A. Ivanov, A. M. Kalashnikova, K. Vahaplar, J. Mentink, A. Kirilyuk, T. Rasing, and A. V. Kimel, Nat. Commun. **3**, 666 (2012).

[2] A. V. Kimel and M. Li, Nat. Rev. Mater. **4**, 189 (2019).

[3] S. Schlauderer, C. Lange, S. Baierl, T. Ebnet, C. P. Schmid, D. C. Valovcin, A. K. Zvezdin, A. V. Kimel, R. V. Mikhaylovskiy, and R. Huber, Nature (London) **569**, 383 (2019).

[4] S. Mangin, M. Gottwald, C.-H. Lambert, D. Steil, V. Uhlíř, L. Pang, M. Hehn, S. Alebrand, M. Cinchetti, G. Malinowski, Y. Fainman, M. Aeschlimann, and E. E. Fullerton, Nat. Mater. **13**, 286 (2014).

[5] R. John, M. Berritta, D. Hinzke, C. Müller, T. Santos, H. Ulrichs, P. Nieves, J. Walowski, R. Mondal, O. Chubykalo-Fesenko, J. McCord, P. M. Oppeneer, U. Nowak, and M. Münzenberg, Sci. Rep. **7**, 4114 (2017).

[6] C.-H. Lambert, S. Mangin, B. S. D. C. S. Varaprasad, Y. K. Takahashi, M. Hehn, M. Cinchetti, G. Malinowski, K. Hono, Y. Fainman, M. Aeschlimann, and E. E. Fullerton, Science **345**, 1337 (2014).

[7] A. Stupakiewicz, K. Szerenos, D. Afanasiev, A. Kirilyuk, and A. V. Kimel, Nature (London) **542**, 71 (2017).

[8] N. A. Spaldin and R. Ramesh, Nat. Mater **18**, 203 (2019).

[9] H. Katsura, N. Nagaosa, and A. V. Balatsky, Phys. Rev. Lett. **95**, 057205 (2005).

[10] I. A. Sergienko and E. Dagotto, Phys. Rev. B **73**, 094434 (2006).

[11] S. L. Johnson, R. A. de Souza, U. Staub, P. Beaud, E. Möhr-Vorobeva, G. Ingold, A. Caviezel, V. Scagnoli, W. F. Schlotter, J. J. Turner, O. Krupin, W.-S. Lee, Y.-D. Chuang, L. Patthey, R. G. Moore, D. Lu, M. Yi, P. S. Kirchmann, M. Trigo, P. Denes *et al.*, Phys. Rev. Lett. **108**, 037203 (2012).

[12] J. A. Johnson, T. Kubacka, M. C. Hoffmann, C. Vicario, S. de Jong, P. Beaud, S. Grübel, S.-W. Huang, L. Huber, Y. W. Windsor, E. M. Bothschafter, L. Rettig, M. Ramakrishnan, A. Alberca, L. Patthey, Y.-D. Chuang, J. J. Turner, G. L. Dakovski, W.-S. Lee, M. P. Minitti *et al.*, Phys. Rev. B **92**, 184429 (2015).

[13] E. M. Bothschafter, E. Abreu, L. Rettig, T. Kubacka, S. Parchenko, M. Porer, C. Dornes, Y. W. Windsor, M. Ramakrishnan, A. Alberca, S. Manz, J. Saari, S. M. Koohpayeh, M. Fiebig, T. Forrest, P. Werner, S. S. Dhesi, S. L. Johnson, and U. Staub, Phys. Rev. B **96**, 184414 (2017).

[14] Y. Yamasaki, S. Miyasaka, Y. Kaneko, J.-P. He, T. Arima, and Y. Tokura, Phys. Rev. Lett. **96**, 207204 (2006).

[15] S. Bordács, D. Varjas, I. Kézsmárki, G. Mihály, L. Baldassarre, A. Abouelsayed, C. A. Kuntscher, K. Ohgushi, and Y. Tokura, Phys. Rev. Lett. **103**, 077205 (2009).

[16] D. H. Lyons, T. A. Kaplan, K. Dwight, and N. Menyuk, Phys. Rev. **126**, 540 (1962).

[17] R. Kumar, R. Padam, S. Rayaprol, V. Siruguri, and D. Pal, J. Appl. Phys. **119**, 123903 (2016).

[18] K. Tomiyasu, J. Fukunaga, and H. Suzuki, Phys. Rev. B **70**, 214434 (2004).

[19] N. Menyuk, K. Dwight, and A. Wold, J. Phys. **25**, 528 (1964).

[20] J. A. Heuver, A. Scaramucci, Y. Blickenstorfer, S. Matzen, N. A. Spaldin, C. Ederer, and B. Noheda, Phys. Rev. B **92**, 214429 (2015).

[21] Y. W. Windsor, C. Piamonteze, M. Ramakrishnan, A. Scaramucci, L. Rettig, J. A. Huever, E. M. Bothschafter, N. S. Bingham, A. Alberca, S. R. V. Avula, B. Noheda, and U. Staub, Phys. Rev. B **95**, 224413 (2017).

[22] N. Ortiz Hernández, S. Parchenko, J. R. L. Mardegan, M. Porer, E. Schierle, E. Weschke, M. Ramakrishnan, M. Radovic, J. A. Heuver, B. Noheda, N. Daffé, J. Dreiser, H. Ueda, and U. Staub, Phys. Rev. B **103**, 085123 (2021).

[23] U. Staub, V. Scagnoli, Y. Bodenthin, M. García-Fernández, R. Wetter, A. M. Mulders, H. Grimmer, and M. Horisberger, J. Synchrotron Rad. **15**, 469 (2008).

[24] U. Flechsig, F. Nolting, A. Fraile Rodríguez, J. Krempaský, C. Quitmann, T. Schmidt, S. Spielmann, and D. Zimoch, AIP Conf. Proc. **1234**, 319 (2010).

[25] K. Holldack, J. Bahrdt, A. Balzer, U. Bovensiepen, M. Brzhezinskaya, A. Erko, A. Eschenlohr, R. Follath, A. Firsov, W. Frentrup, L. Le Guyader, T. Kachel, P. Kuske, R. Mitzner, R. Müller, N. Pontius, T. Quast, I. Radu, J.-S. Schmidt, C. Schüßler-Langeheine *et al.*, J. Synchrotron Rad. **21**, 1090 (2014).

[26] P. Choudhary, A. Yadav, and D. Varshney, AIP Conf. Proc. **1832**, 050051 (2017).
[27] J. Stöhr, J. Magn. Magn. Mater. **200**, 470 (1999).
[28] J. Als-Nielsen and D. McMorrow, *Elements of Modern X-ray Physics: Als-Nielsen/Elements* (John Wiley & Sons, Hoboken, 2011).
[29] D. Kamenskyi, H. Engelkamp, T. Fischer, M. Uhlarz, J. Wosnitza, B. P. Gorshunov, G. A. Komandin, A. S. Prokhorov, M. Dressel, A. A. Bush, V. I. Torgashev, and A. V. Pronin, Phys. Rev. B **87**, 134423 (2013).
[30] T. Ogasawara, K. Ohgushi, Y. Tomioka, K. S. Takahashi, H. Okamoto, M. Kawasaki, and Y. Tokura, Phys. Rev. Lett. **94**, 087202 (2005).
[31] X. Wang, S. Nie, J. Li, R. Clinite, J. E. Clark, and J. Cao, Phys. Rev. B **81**, 220301(R) (2010).
[32] A. Manchon, Q. Li, L. Xu, and S. Zhang, Phys. Rev. B **85**, 064408 (2012).
[33] M. Sultan, U. Atxitia, A. Melnikov, O. Chubykalo-Fesenko, and U. Bovensiepen, Phys. Rev. B **85**, 184407 (2012).
[34] J. Kimling, J. Kimling, R. B. Wilson, B. Hebler, M. Albrecht, and D. G. Cahill, Phys. Rev. B **90**, 224408 (2014).
[35] T. Roth, A. J. Schellekens, S. Alebrand, O. Schmitt, D. Steil, B. Koopmans, M. Cinchetti, and M. Aeschlimann, Phys. Rev. X **2**, 021006 (2012).
[36] R. D. Averitt, A. I. Lobad, C. Kwon, S. A. Trugman, V. K. Thorsmølle, and A. J. Taylor, Phys. Rev. Lett. **87**, 017401 (2001).
[37] A. Kirilyuk, A. V. Kimel, and T. Rasing, Rev. Mod. Phys. **82**, 2731 (2010).
[38] R. Guzman, J. Heuver, S. Matzen, C. Magén, and B. Noheda, Phys. Rev. B **96**, 104105 (2017).
[39] W. Töws and G. M. Pastor, Phys. Rev. B **100**, 024402 (2019).
[40] G. Lawes, B. Melot, K. Page, C. Ederer, M. A. Hayward, T. Proffen, and R. Seshadri, Phys. Rev. B **74**, 024413 (2006).
[41] D. Das, R. Biswas, and S. Ghosh, J. Phys.: Condens. Matter **28**, 446001 (2016).
[42] T. Ferté, N. Bergeard, L. Le Guyader, M. Hehn, G. Malinowski, E. Terrier, E. Otero, K. Holldack, N. Pontius, and C. Boeglin, Phys. Rev. B **96**, 134303 (2017).
[43] I. Radu, K. Vahaplar, C. Stamm, T. Kachel, N. Pontius, H. A. Dürr, T. A. Ostler, J. Barker, R. F. L. Evans, R. W. Chantrell, A. Tsukamoto, A. Itoh, A. Kirilyuk, T. Rasing, and A. V. Kimel, Nature (London) **472**, 205 (2011).
[44] A. D. Caviglia, M. Först, R. Scherwitzl, V. Khanna, H. Bromberger, R. Mankowsky, R. Singla, Y.-D. Chuang, W. S. Lee, O. Krupin, W. F. Schlotter, J. J. Turner, G. L. Dakovski, M. P. Minitti, J. Robinson, V. Scagnoli, S. B. Wilkins, S. A. Cavill, M. Gibert, S. Gariglio *et al.*, Phys. Rev. B **88**, 220401(R) (2013).
[45] B. Koopmans, G. Malinowski, F. Dalla Longa, D. Steiauf, M. Fähnle, T. Roth, M. Cinchetti, and M. Aeschlimann, Nat. Mater. **9**, 259 (2010).
[46] D. Talbayev, J. Lee, S. A. Trugman, C. L. Zhang, S.-W. Cheong, R. D. Averitt, A. J. Taylor, and R. P. Prasankumar, Phys. Rev. B **91**, 064420 (2015).
[47] I. P. Handayani, R. I. Tobey, J. Janusonis, D. A. Mazurenko, N. Mufti, A. A. Nugroho, M. O. Tjia, T. T. M. Palstra, and P. H. M. van Loosdrecht, J. Phys.: Condens. Matter **25**, 116007 (2013).
[48] H. C. Shih, L. Y. Chen, C. W. Luo, K. H. Wu, J.-Y. Lin, J. Y. Juang, T. M. Uen, J. M. Lee, J. M. Chen, and T. Kobayashi, New J. Phys. **13**, 053003 (2011).
[49] A. Sethi, T. Byrum, R. D. McAuliffe, S. L. Gleason, J. E. Slimak, D. P. Shoemaker, and S. L. Cooper, Phys. Rev. B **95**, 174413 (2017).
[50] http://doi.psi.ch/detail/10.16907%2F200707de-2b6f-490e-813b-5e7b069270fe.